PAPER

Check for updates

Deciphering the role of LiBr as a redox mediator in Li–O₂ aprotic batteries

Angelica Petrongari, [ID] [a] Lucrezia Desiderio,[a] Adriano Pierini,[a] Enrico Bodo [ID] [a] Mauro Giustini [ID] [a] and Sergio Brutti [ID] *[abc]

Lithium–oxygen batteries (Li–O₂) represent a highly promising category of energy storage systems, primarily owing to their elevated theoretical energy density. Nevertheless, their effective deployment is significantly impeded by challenges such as inadequate reversibility and the presence of undesirable parasitic reactions. Recent investigations have turned to redox mediators, specifically lithium bromide (LiBr), as a potential solution to improve reaction kinetics and minimize overpotentials in these systems. This research presents a comprehensive analysis of the effects of three distinct solvents – dimethoxyethane (DME), tetraethylene glycol dimethyl ether (TEGDME), and dimethyl sulfoxide (DMSO) – on both the electrochemical performance and reaction mechanisms of LiBr-mediated lithium–oxygen cells. The findings indicate that singlet oxygen ($^1O_2$), which contributes to cell degradation through secondary reactions, is generated only in the presence of TEGDME as the electrolyte solvent. In contrast, while both DME and DMSO enable oxygen evolution without forming singlet oxygen, only DME exhibits chemical stability under the operating conditions of LiBr-mediated Li–O₂ cells. Furthermore, a comparative analysis of the redox mediation effects arising from lithium iodide (LiI) and LiBr across various solvent environments reveals that the activation of the singlet oxygen release pathway occurs when the Lewis acidity and basicity of the oxidized redox mediator and the solvent are aligned—for example, when both behave as weak acids/bases or as strong acids/bases. This study elucidates the nuanced interactions between solvents and redox mediators, thereby contributing to the advancement of more efficient lithium–oxygen battery systems.

Introduction

Aprotic Li–O₂ batteries are considered a promising technology to address the increasing demand for energy storage systems. These devices can potentially deliver outstanding performance thanks to their gravimetric energy density (up to 3458 Wh per kg with Li₂O₂ as the discharge product) and high operating potential (*i.e.* 2.96 V *vs.* Li⁺/Li⁰).[1] The redox processes involved in the functioning of a Li–O₂ cell are the dissolution (discharge) and deposition (charge) of lithium at the lithium metal anode and the Oxygen Reduction Reaction (ORR, discharge) and Oxygen Evolution Reaction (OER, charge) at the carbonaceous cathode. In aprotic electrolytes, the ORR and OER lead to the formation and dissolution, respectively, of the non-conductive solid lithium peroxide.[2]

Some key drawbacks must be faced before achieving the practical implementation of these systems: in particular, the

high overpotentials required during the charge process, *i.e.* the oxidation of lithium peroxide to molecular oxygen, must be efficiently lowered to avoid undesired processes that lead to early performance decay of the cell.[3,4] Among the strategies to suppress singlet oxygen ($^1O_2$) in Li–O₂ batteries, quenching mechanisms have been explored. Molecules such as triphenylamine (TPA) and its brominated derivative can capture $^1O_2$ and convert it to ground-state oxygen, effectively reducing parasitic reactions and improving battery stability.[5,6] Another effective method to avoid singlet oxygen production is to introduce soluble catalysts named Redox Mediators (RMs), which are currently being explored and proposed in the literature to favour the oxidation of Li₂O₂ at lower overpotentials and preserve the cell components from degradation.[7,8] RMs are oxidized at the cathode surface and then diffuse to Li₂O₂ deposits where they oxidize the peroxide anion to molecular oxygen, acting as electron carriers and allowing the lowering of the charge potential.[9]

Adding lithium halides, LiX, to the electrolyte solution is a promising and cost-effective strategy to employ the redox couples of halide species, in particular X^-/X_3^- and X_3^-/X_2, as redox mediators.[10] LiI is a widely studied RM that shows interesting results,[11,12] although it also raises additional concerns

[a]Department of Chemistry, Sapienza University of Rome, P.le Aldo Moro 5, Rome, 00185, Italy. E-mail: sergio.brutti@uniroma1.it

[b]CNR-ISC, Consiglio Nazionale delle Ricerche, Istituto dei Sistemi Complessi, Rome, 00185, Italy

[c]GISEL – Centro di Riferimento Nazionale per i Sistemi di Accumulo Elettrochimico di Energia, Florence, 50121, Italy

regarding the stability of cell components.[13] More recently, LiBr was also proposed as an electrolyte salt and redox mediator by Kwak et al.,[14] highlighting some advantages of this RM against LiI: a higher oxidizing power due to the higher standard potential of the redox couple Br^-/Br_3^-; a more efficient formation of Li_2O_2 during discharge and little to no competition between bromide chemistry and the ORR/OER. These differences are consistent with our findings reported in ref. 16, where LiI was tested in the same solvent systems used in the present study for LiBr. In Kwak et al.'s report, LiBr performance was particularly promising when using diglyme (diglyme = diethylene glycol dimethyl ether) as electrolyte solvent, while a decay of the cell performance along with a worsening of the charge/discharge overpotentials was observed using TEGDME as solvent.[14] This behaviour deviates from that observed in the case of LiI,[11] and the fundamental origin of such a different performance outcome when varying between very similar solvents has not been further explained up to now. Based on Pierini et al.'s calculations,[15] we hypothesized that, similarly to the LiI case, the promotion of singlet oxygen release due to the introduction of the RM could be involved. The oxidation of a cluster of $(Li_2O_2)_4$ by Br_3^- was thermodynamically favoured in both highly polar solvents like DMSO and ethereal solvents,[15] suggesting that in the case of LiBr singlet oxygen generation could be favoured also in low-polarity media, in contrast with the case of LiI.

In fact, in a previous study,[16] we observed that the use of LiI coupled with a high-polarity solvent like DMSO, where the oxidation of Li_2O_2 by I_3^- corresponds to a $\Delta G < 0$ (ref. 15), leads to a significant increase of the amount of $^1O_2$ evolved during the oxidation of Li_2O_2 by the redox mediator.

The implications of using LiBr on the degradative processes in the Li–O_2 cell need to be widely explored in order to design an appropriate electrolyte formulation to maximize the performance of this promising RM. With this aim, we carried out a study employing LiBr 200 mM + LiTFSI 1 M in monoglyme (DME)/tetraglyme (TEGDME)/dimethylsulfoxide (DMSO) solvents, to determine the fundamental origin of different performance outcomes within the same class of solvents and the same range of polarity in the case of DME and TEGDME (ε_r = 7.2 and 7.4, respectively[17,18]), and to also highlight the effect of a sharp change in polarity using DMSO (ε_r = 46.8 (ref. 19)). The 200 mM LiBr concentration was chosen to ensure the best reversibility of the ORR/OER processes, as indicated by the preliminary tests reported in Fig. S1.

Materials and methods

Electrolytes

High-purity 1,2-dimethoxyethane (monoglyme; DME) [anhydrous, 99.5%, inhibitor-free], tetraglyme (TEGDME) [tetraethylene glycol dimethyl ether, anhydrous, ≥99%] and dimethyl sulfoxide (DMSO) [Sigma-Aldrich, anhydrous, ≥99%] were purchased from Sigma-Aldrich and dried over 4 Å molecular sieves for at least 1 week before use. Battery grade LiTFSI (lithium bis(trifluoromethanesulfonyl)imide extra dry <20 ppm of H_2O, Solvionic) was used as received. LiBr (Reagent-Plus®,

≥99%, Sigma-Aldrich) was dried under vacuum at 50 °C for 48 h before use. Electrolyte solutions of LiTFSI 1 M + LiBr 200 mM in DME/TEGDME/DMSO were prepared in an Ar filled glovebox (Iteco Eng SGS-30, H_2O <0.1 ppm).

Electrochemical measurements

An EL-CELL ECC-Air test cell was used to perform electrochemical experiments. The internal configuration of the cell employed for all the measurements is as follows: Li(−)/Separator-Electrolyte/GDL(+)/Ni Foam/Gaseous O_2 (1 bar). A glass fiber separator (Whatman, 1.55 mm thickness, 18 mm diameter) soaked in 1 M LiTFSI + 200 mM LiBr in DME/TEGDME/DMSO electrolytes was employed. 15 mm discs of a commercial carbonaceous Gas Diffusion Layer (GDL, MTI Corp.) were used as cathodes. A metallic lithium foil was used as the anode. A nickel foam disc (16 mm diameter) was used above the GDL to ensure a homogeneous O_2 impregnation. Cell assembly was performed in an Ar filled glovebox (Iteco Eng SGS-30, H_2O <0.1 ppm). The Li–O_2 cells were filled with pure O_2, setting a static final pressure of 2.0 bar in the cell volume (head space 4.3 cm^3). Galvanostatic cycling tests were run on (−)Li^0|LiTFSI 1 M + LiBr 200 mM in DME|GDL(+), (−)Li^0|LiTFSI 1 M + LiBr 200 mM in TEGDME|GDL(+) and (−)Li^0|LiTFSI 1 M + LiBr 200 mM in DMSO|GDL(+) cells at 0.1 mA cm^{-2} with a limited capacity of 0.2 mA h cm^{-2} and cut-off potentials of 2.0 and 3.6 V vs. Li$^+$/Li^0, using a Maccor Series 4000 Battery Test System.

Ex situ experiments

The fluorescent probe DMA [9,10-dimethylanthracene, 99%] and bromine (Br$_2$, Suprapur®, 99.9999%) were purchased from Sigma-Aldrich and used as received. A set of reference DMA solutions, at the concentrations of 0.5–1–2.5–5–7.5 and 10 μM, was prepared in each solvent (DME/TEGDME/DMSO) for the construction of the calibration lines. The reaction solutions were prepared in each solvent according to the following scheme:

Solution A: 5.15 mg of 9,10-dimethylanthracene were dissolved in 5 mL of the chosen solvent to obtain a 5 mM solution. The solution was then diluted with the same solvent to 0.2 mM of DMA.

Solution B: 10 μL of pure Br$_2$ and 33.7 mg of dry LiBr were added to 4.85 mL of the chosen solvent to obtain a 40 mM solution of Br$_3^-$. The solution was then diluted with the same solvent to 0.2 mM.

Equal volumes of solutions A and B were mixed to obtain a 0.1 mM solution of both Br$_3^-$ and DMA. A portion of the as-prepared solution was further diluted 10× and its fluorescence and UV spectra were recorded as references before adding Li_2O_2. Excess Li_2O_2 was added to the other portion of the A + B solution to perform Li_2O_2 oxidation with Br$_3^-$ in the presence of a 1 : 1 quantity of DMA as a singlet oxygen trap, and then the final solution was diluted 10× and its fluorescence and UV spectra were recorded. The preparation of both the reference and the reaction solutions was carried out under an Ar atmosphere in a MBRAUN UniLab glovebox [H_2O, O_2 ≤1 ppm].

The measurements were carried out in sealable Hellma quartz fluorescence cuvettes 117104F-10-40, to prevent the

This journal is © The Royal Society of Chemistry 2026

J. Mater. Chem. A, 2026, **14**, 560–569 | **561**

exposure of the solutions to air moisture and oxygen. Fluorescence measurements were performed with a Fluoromax-2 spectrofluorometer (Jobin Yvon-Spex), in the 392–600 nm range with an excitation wavelength of 388 nm (slits 1.1/1.1 nm) and at a temperature of 25 °C. UV spectra were recorded with a Varian Cary 5E UV-Vis spectrophotometer. Sealable fluorescence quartz cuvettes were also employed for the acquisition of Raman spectra.

Spectra of the 40 mM solution of Br_3^- before and after adding Li_2O_2 were recorded in TEGDME and DMSO as solvents. Raman measurements were carried out with a DILOR LabRam confocal micro-Raman equipped with a He–Ne laser source at 632.7 nm.

Computational details

Simulations of Raman spectra of Br_3^- and Br_2 were carried out using density functional theory (DFT) at the M062X/def2-TZVP level. Simulations of FTIR spectra of dimethyl sulfide and methanesulfonic acid were carried out by DFT at the wB97X/def2-TZVPP,[20] NoFrozenCore level of theory, with the Orca package distribution, version 5.03.[21]

Results

LiBr redox mediation in DME

When charged up to 3.6 V with no limit capacity (Fig. S1b), the Li–O_2 cell containing LiTFSI 1 M + LiBr 200 mM in DME shows a charge profile closely matching the discharge, indicating good reversibility and efficient utilization of the redox mediator under these conditions. Moving to prolonged cycling conditions, the charge/discharge capacities achieved during the galvanostatic cycling of the same cell formulation with a limited capacity of 0.2 mAh cm^{-2} at J = 0.1 mA cm^{-2} are reported in Fig. 1a. This electrolyte formulation allows a stable functioning of the LiBr-mediated cell, with an excellent reversibility of the ORR/OER for at least 60 cycles. In line with this, the potential curves reported in Fig. 1b indicate both a good discharge profile and a low-overpotential, stable charge performance. Only after 50 cycles, a mild worsening of the discharge process is observed,

as indicated by the higher overpotential at which the 50th discharge takes place, likely due to a reduced oxygen concentration at the reaction interface caused by cumulative minor irreversibilities. The slight shift of the discharge plateau towards higher capacities observed in the 10th and 50th discharges is likely due to a moderate accumulation of Br_3^- during charge, which is by consequence reduced in correspondence with the very early stages of discharge at higher potentials than 2.75 V (*i.e.* the ORR onset). It is important to underline that in the case of the use of LiI as the redox mediator, the impact of the I_3^- accumulation is large,[22] while it is almost negligible in the case of LiBr mediation. This aspect indicates that LiBr offers better performance in ethereal solvents, thanks to the very high overpotentials required for the reduction of Br_3^- on the carbon cathode that make this process non-competitive with the ORR during discharge. On passing, we would like to stress that, although the technological validation of this electrolyte formulation for Li–O_2 necessarily requires much more extended cycling in terms of limiting current/capacities and cycle number, here our goal is to demonstrate the fundamental behaviour of LiBr as a redox mediator in three different solvent media. In this respect, the presented galvanostatic tests, even if limited to 60 cycles, offer a solid experimental basis to prove in which chemical environments LiBr drives or limits parasitic degradation reactivities. This experimental validation aims at consolidating our hypothesis that redox mediators and electrolytes are strongly interplayed and the impact of solvation on the thermodynamics and kinetics of redox mediation is not banal and cannot be fully explained by simple considerations starting from the acceptor/donor numbers of solvents. The good stability of the electrochemical performance of LiBr in DME suggests that this electrolyte formulation leads to limited parasitic chemistries and the possible suppression of $^1O_2$ release beyond the quantities expected by the Boltzmann distribution, as calculated in eqn (S1). To confirm this hypothesis, an *ex situ* study on the oxidation of Li_2O_2 by Br_3^- in DME was performed. Excess Li_2O_2 was added to a 0.1 mM solution of Br_3^- in DME, in the presence of 0.1 mM of DMA (the $^1O_2$ trap). The reaction solution was then diluted to
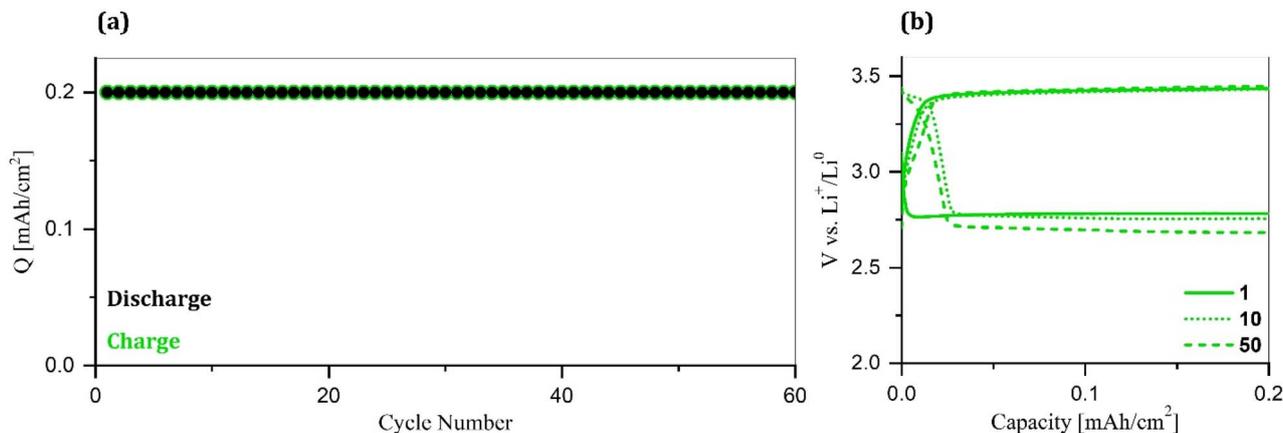

Fig. 1 (a) Discharge/charge capacities achieved by a Li–O_2 cell with LiTFSI 1 M + LiBr 200 mM in DME electrolyte, cycled at J = 0.1 mA cm^{-2}, Q_{lim} = 0.2 mAh cm^{-2}, and $V_{cut-off}$ = 2.0–3.6 V *vs.* Li$^+$/Li^0, for 60 cycles. (b) Voltage profiles of the 1st, 10th and 50th cycles.

562 | *J. Mater. Chem. A*, 2026, **14**, 560–569

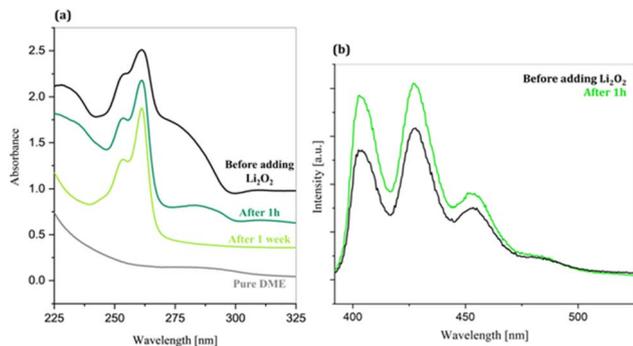This journal is © The Royal Society of Chemistry 2026

Fig. 2 (a) UV spectra of pure DME (grey) and a solution of Br_2 10 μM + LiBr 40 μM + DMA 10 μM in DME before (black) and after (1 h, dark green and 1 week, light green) adding excess Li_2O_2. (b) Fluorescence spectra of a solution of Br_2 10 μM + LiBr 40 μM + DMA 10 μM in DME before (black) and after (green) adding excess Li_2O_2.

0.01 mM in order to record its UV and fluorescence spectra. Simultaneously, another aliquot of the initial solution was diluted to 0.01 mM (of Br_3^- and DMA) and its UV and fluorescence spectra were recorded as a reference of the spectral response of the solution before adding Li_2O_2. Fig. 2a illustrates the UV spectra of the reaction solution before adding Li_2O_2 and after 1 h and 1 week. The baseline of pure DME is reported as a blank. The UV signal of Br_3^- is localized at ~280 nm: this position is assigned by comparison with the shape and position of the Br_3^- UV signal in aqueous solution observed in the literature.[23] One hour after the addition of Li_2O_2, a sharp decrease of the Br_3^- signal can be observed, indicating its consumption in the oxidation reaction with lithium peroxide.

The complete disappearance of the Br_3^--related signal is observed 1 week after the onset of the reaction. The UV spectral response during the Li_2O_2 oxidation by Br_3^- in DME highlights that not only is the reaction spontaneous but also occurs with relatively fast kinetics. It is worth mentioning that when LiI is used as the RM, the oxidation of Li_2O_2 in glymes is either not spontaneous[15] or strongly kinetically hindered,[12] while in the case of LiBr the analogous reaction is thermodynamically as supported by both theoretical calculations[15] and experimental

evidence. Additionally, the Li_2O_2 oxidation by Br_3^- in DME occurs without the evolution of $^1O_2$, as indicated by the comparison of DMA fluorescence spectra before and after adding Li_2O_2 (Fig. 2b). In fact, the increase in the fluorescence signal of DMA observed after adding Li_2O_2 was demonstrated to result solely from an interaction between DMA and Li_2O_2, with no contribution of the OER mediated by Br_3^- to the intensity variation of the DMA spectrum. When excess Li_2O_2 is added to a 10 μM solution of DMA in DME (Fig. S2), the same increase in intensity is observed (see Table S1).

LiBr redox mediation in TEGDME

LiBr performance as a redox mediator in TEGDME was first studied by Kwak et al.,[14] who had already observed the worsening of the cell operation in this solvent compared to the shorter-chain diglyme. The observations discussed in the previous paragraph for DME as battery solvent are in line with the picture that emerges from the work of Kwak et al. Overall, it appears that both DME and diglyme (DEGDME), which differ by only a $-O-(CH_2)_2-$ unit, are suitable solvents for LiBr employment, while earlier performance decay is to be expected for longer chain glymes such as TEGDME. This marked performance difference within the same class of solvents is specific to LiBr and was not observed in the case of LiI, nor for many other RMs.[24] In Fig. 3, the electrochemical behaviour of a Li–O$_2$ cell containing LiTFSI 1 M + LiBr 200 mM in TEGDME as electrolyte, cycled at $J = 0.1$ mA cm^{-2} $Q_{lim} = 0.2$ mAh cm^{-2} between 2.0 and 3.6 V vs. Li$^+$/Li^0, is reported. Early failure of the charge process is observed starting from cycle 12, from which the charge capacities continuously decrease (Fig. 3a). The charge/discharge potential profiles shown in Fig. 3b highlight the occurrence of critical parasitic chemistries: in the 10th cycle, the contribution of the Br$^-$ redox to the discharge capacity extends to almost half of the total capacity, indicating that accumulation of Br_3^- during charge due to inefficient redox mediation occurs. In the 50th cycle, a three-plateau discharge profile is observed. The first plateau at ~3.4 V, which is related to excess Br_3^- reduction, is less extended than in the 10th discharge; however, the ORR-related plateau at ~2.7 V is shorter due to the presence of a third
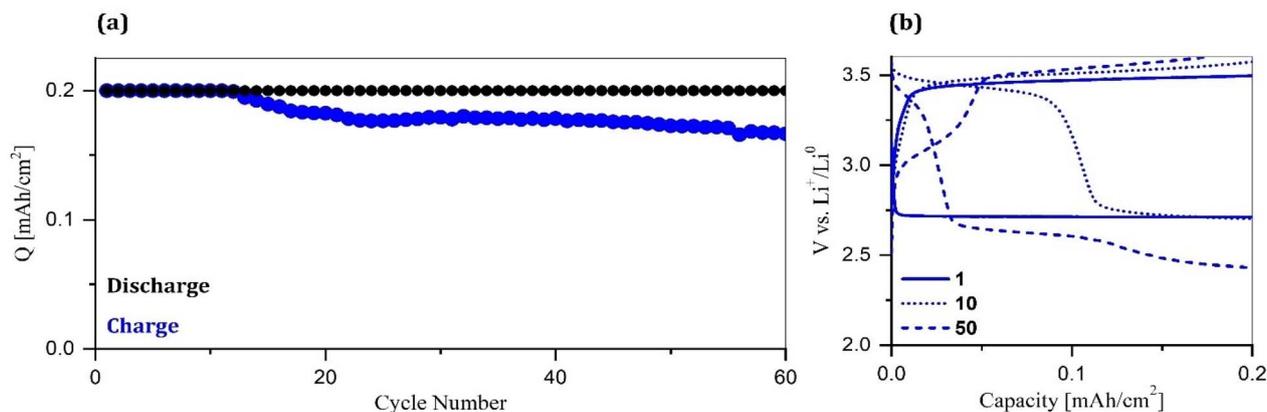

Fig. 3 (a) Discharge/charge capacities achieved by a Li–O$_2$ cell with the LiTFSI 1 M + LiBr 200 mM in TEGDME electrolyte, cycled at $J = 0.1$ mA cm^{-2}, $Q_{lim} = 0.2$ mAh cm^{-2}, and $V_{cut-off} = 2.0$–3.6 V vs. Li$^+$/Li^0 for 60 cycles. (b) Voltage profiles of the 1st, 10th and 50th cycles.

This journal is © The Royal Society of Chemistry 2026

J. Mater. Chem. A, 2026, 14, 560–569 | 563

plateau at ~2.4 V, hinting that additional undesired processes are occurring alongside the ORR. Observing the charge profiles, it appears that in the 10th charge only an increase in over-potential occurred, while a radical change in the electro-chemical process is evident in the 50th cycle.

Such differences between the performance outcomes in DME and TEGDME may indicate that, despite the identical class of ethereal solvents, the $^1O_2$ evolution channel activates in the solvent, *i.e.* TEGDME, that has a slightly larger dielectric constant and a slightly smaller acceptor number. The *ex situ* experiments performed to understand the fundamentals of LiBr mediation in TEGDME are reported in Fig. 4. When the reaction solution (40 mM Br_3^- + 40 mM DMA + excess Li_2O_2 in TEGDME) was monitored over time by Raman spectroscopy, the consumption of Br_3^- was confirmed (Fig. 4a): a monotone decrease in the Raman Br_3^- signal intensity centered at 175 cm^{-1} is evident, strongly indicating that the oxidation of Li_2O_2 has occurred. The assignment of the peak at 175 cm^{-1} to $LiBr_3$ is confirmed by both the literature (ref. 10) and theoretical calculations (Fig. S3). In Fig. 4b, the fluorescence spectra of the singlet oxygen trap DMA before and after adding Li_2O_2 in the reaction solution of Br_3^- 0.1 mM + DMA 0.1 mM in TEGDME are reported. A decrease of the fluorescence intensity indicates that part of the DMA in solution reacted with $^1O_2$ forming the non-fluorescent DMA-endoperoxide.

From the calibration plot reported in Fig. S4, it was possible to estimate that the amount of DMA that reacted with $^1O_2$ was around 1.9% of the initial concentration. The 1 : 1 reaction stoichiometry between DMA and $^1O_2$, in forming DMA-endoperoxide, therefore implies that at least ~1.9% of the total molecular oxygen evolved in its singlet state. This result is comparable with that obtained for LiI redox mediation in DMSO reported in our previous study[16] and demonstrates that LiBr is also able to open an alternative pathway for $^1O_2$ evolution enabling its production far beyond the quantities expected from the Boltzmann distribution. Apparently, the key difference lies in the interplay between polarity (dielectric constant) and the Lewis acidity (acceptor number) of the solvent and the Lewis

basicity of the redox mediator. LiI is the precursor of the strong Lewis base I_3^- and it leads to $^1O_2$ generation only in a high-polarity solvent, DMSO, that is a strong Lewis acid with a large acceptor number. In a low polarity/weak Lewis acid solvent like TEGDME, LiI mediates a $^1O_2$-free Li_2O_2 oxidation. In contrast, LiBr is the precursor of the weak Lewis base Br_3^- and activates the release of singlet oxygen in a low-polarity solvent, TEGDME, that is a weak Lewis acid, whereas in DME, a low polarity solvent but with intermediate Lewis acidity (*i.e.* acceptor number intermediate between TEGDME and DMSO) the Li_2O_2 oxidation mediated by LiBr is $^1O_2$-free.

LiBr redox mediation in DMSO

A different behaviour of LiBr-mediated Li–O_2 batteries is observed when DMSO is used as electrolyte solvent. In Fig. 5, the cycling performance of a Li–O_2 cell with LiTFSI 1 M + LiBr 200 mM in DMSO is reported. Already starting from the 18th cycle (Fig. 5a), the discharge process becomes inefficient, likely due to the lack of molecular oxygen in the cell head compartment. The scarcity of oxygen supply may derive from an ineffi-cient charging process, as can be deduced by the shape of the charge potential profiles of the first cycles (Fig. 5b), indicating the onset of a parasitic process activated at ~3.6 V. Based on the observation of the preliminary electrochemical tests with no limit capacity (Fig. S5), it appears that this process involves not only the oxidations of Br^- to Br_3^- and Li_2O_2 to O_2, but also the oxidation of electrolyte components, hindering the actual OER. As a consequence, the accumulation of Br_3^- (or Br_2) occurs cycle by cycle due to the progressive lack of Li_2O_2 formed during discharge. We can speculate that the high polarity of DMSO allows the involvement of the second redox couple of LiBr within the potential window employed for the galvanostatic cycling of the cell, *i.e.* 2.0–3.6 V *vs.* Li$^+$/Li^0, with the oxidation of Br_3^- to Br_2 occurring at ~3.6 V. In fact, it was observed that this reaction occurs at lower potential in DMSO (3.9 V) than in ethers (4.1 V)[9] in an Ar atmosphere, and since these values are further lowered in the presence of O_2 (ref. 14) it is reasonable that the Br_3^-/Br_2 oxidation is the process occurring at ~3.6 V in the charge profiles reported in Fig. 5b. Qualitatively, it was observed that, upon the recovering and washing of the cathodes, only the one cycled in DMSO caused the fresh solvent to turn orange (Fig. S6), supporting the presence of high quantities of Br_2 in the electrolyte after the cycling procedure. Once formed, Br_2 is able to decompose DMSO to dimethyl sulfide, formaldehyde and methanesulfonic acid, according to the scheme elucidated by Aida *et al.*[25]

Based on these evaluations, it is likely that the short cycle life of the Li–O_2 cell cycled with the DMSO-based electrolyte can be safely attributed to the chemical instability of DMSO in the presence of Br_2. Although the production of $^1O_2$ is in this case reasonable due to the theoretical predictions,[15] it has to be kept in mind that the oxidizing power of Br_2 towards the solvent and the Li salt may also be the most relevant aspect leading to cell failure.

The *ex situ* experiments performed to study the oxidation of Li_2O_2 by Br_3^- in DMSO are reported in Fig. 6.
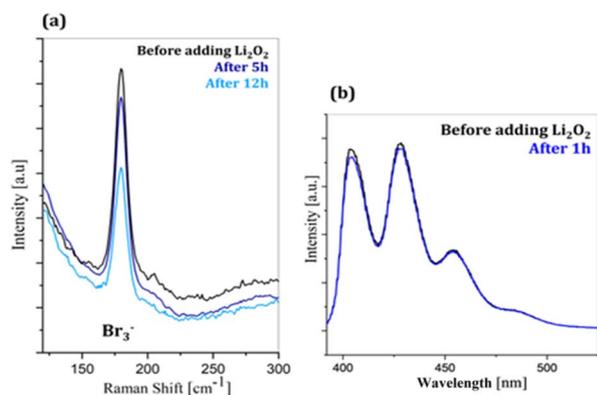

Fig. 4 (a) Raman spectra of a solution of Br_3^- 40 mM in TEGDME before adding excess Li_2O_2, after 5 hours (dark blue) and after 12 hours (light blue). (b) Fluorescence spectra of DMA before (black) and after 1 hour (blue) of adding Li_2O_2 to the reaction solution of 0.1 mM Br_3^- + 0.1 mM DMA.
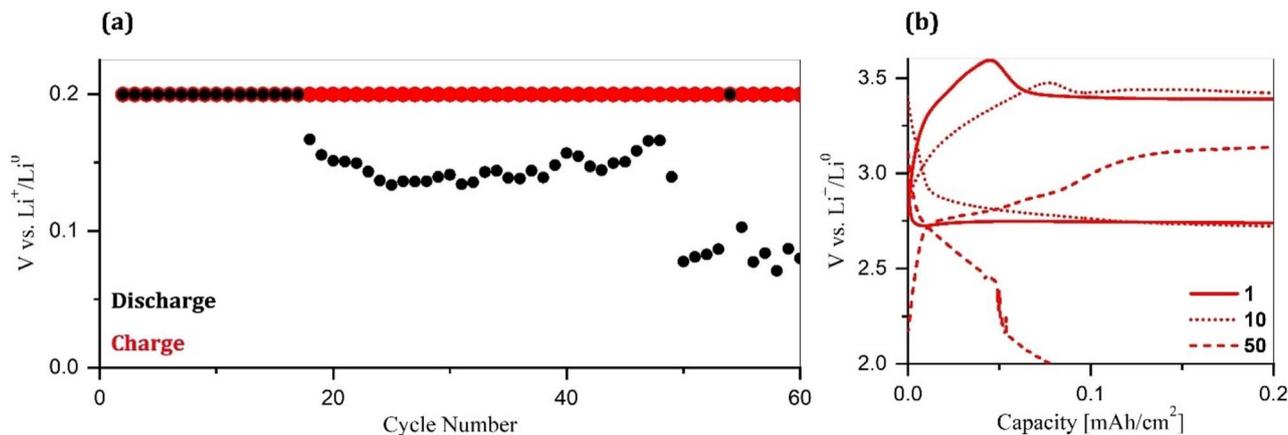
564 | *J. Mater. Chem. A*, 2026, **14**, 560–569

This journal is © The Royal Society of Chemistry 2026

Fig. 5 (a) Discharge/charge capacities achieved by a Li–O$_2$ cell with the LiTFSI 1 M + LiBr 200 mM in DMSO electrolyte, cycled at $J = 0.1$ mA cm^{-2}, $Q_{lim} = 0.2$ mAh cm^{-2}, and $V_{cut-off} = 2.0$–3.6 V vs. Li$^+$/Li^0 for 60 cycles. (b) Voltage profiles of the 1st, 10th and 50th cycles.

In Fig. 6a, the presence of the Br$_3^-$ Raman signal before adding Li$_2$O$_2$ is evident. Its band shape is significantly different from that observed in ethers (see Fig. 4a) and has the typical broad aspect of the Br$_2$ signal (Fig. S3), which is likely because the Br$_3^-$ species exists mainly as a Br$_2^+$Br$^-$ complex. In the Fig. 6a it is possibile to observe that the consumption of Br$_3^-$ is complete in a few minutes from the reaction onset, indicating a very fast kinetics of the Li$_2$O$_2$ oxidation by Br$_3^-$ (or Br$_2$) in DMSO. In Fig. 6b are reported the DMA fluorescence spectra for the 1 : 1 reaction mixture with Br$_3^-$ in DMSO before and after the addition of an excess of Li$_2$O$_2$, clearly indicating that the Li$_2$O$_2$ oxidation is not accompanied by singlet oxygen evolution in this case. In fact, the fluorescence intensity of DMA is not affected by the occurrence of the reaction. This result is in perfect agreement with our previous considerations about the apparent need for a match between the Lewis character of the RM and the electrolyte solvent despite its polarity: DMSO is a strong Lewis acid characterized by a large acceptor number whereas Br$_3^-$ is a weak Lewis base. Overall, LiBr redox mediation in DMSO, a high polarity solvent, seems to follow an alternative mechanism compared to low polarity ethers, which allows ^{1}O$_2$-free Li$_2$O$_2$ oxidation. In the case of DMSO, however,

the performance outcome of LiBr as a RM remains unsuccessful due to the solvent instability and to the formation during the charge not only of Br$_3^-$, but also of the more oxidizing Br$_2$.

Post-mortem characterization of the positive electrodes

Fig. 7 reports the SEM images and corresponding EDX mapping of the gas diffusion layers after their cycling in the DME, TEGDME and DMSO based electrolyte formulations, which will be referred to as GDL$_{(DME)}$, GDL$_{(TEGDME)}$ and GDL$_{(DMSO)}$, respectively.
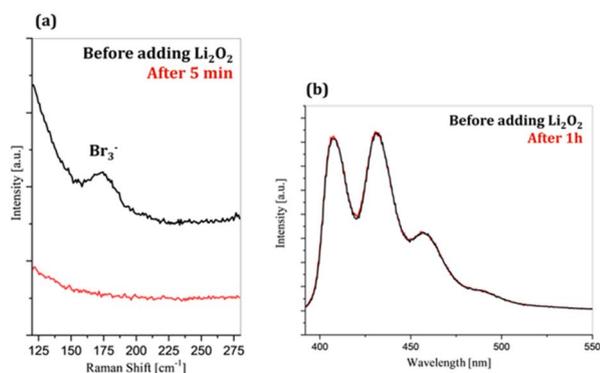

Fig. 6 (a) Raman spectra of a solution of 40 mM Br$_3^-$ in DMSO before (black) and after 5 minutes (red) from adding excess Li$_2$O$_2$. (b) Fluorescence spectra of DMA before (black) and after 1 hour (red) from adding Li$_2$O$_2$ to the reaction solution of 0.1 mM Br$_3^-$ + 0.1 mM DMA.
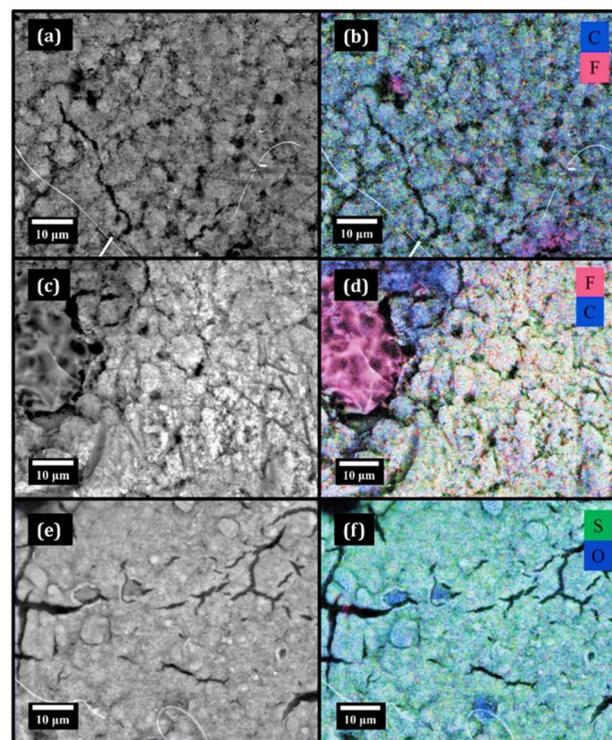
Fig. 7 Scanning electron microscopy images (5.000× magnification, working distance of 8.44 mm, 15 kV electron beam energy) of (a) GDL$_{(DME)}$, (c) GDL$_{(TEGDME)}$, and (e) GDL$_{(DMSO)}$. Corresponding EDX elemental mapping of (b) GDL$_{(DME)}$, (d) GDL$_{(TEGDME)}$, and (f) GDL$_{(DMSO)}$.

Table 1 EDX elemental quantitative analysis of gas diffusion layers cycled with different electrolyte formulations

Sample	Atomic%				
	C	O	S	F	Ni
GDL$_{(DME)}$	45.29	32.42	3.78	13.11	3.32
GDL$_{(TEGDME)}$	15.84	51.62	1.07	24.07	4.67
GDL$_{(DMSO)}$	24.72	53.19	13.10	6.48	1.64

In line with the electrochemical observations, GDL$_{(DME)}$ (Fig. 7a and b) maintains a good morphology after cycling, similar to that of the pristine GDL (Fig. S7), along with a clean surface free of significant deposits of degradation products. In fact, the EDX elemental mapping reported in Fig. 7b and the corresponding quantitative analysis (Table 1) indicate carbon as the main component, with small amounts of fluorine and sulfur that likely derive from the moderate degradation of the TFSI⁻ anion. GDL$_{(DME)}$ composition deviates less than the other postmortem samples compared to the composition of the pristine GDL (Table S2). The main difference lies in the oxygen content, which increased after cycling, consistent with the formation of a natural cathode–electrolyte interphase (CEI) formed from DME derivatives.

This picture is further supported by the ATR-FTIR spectrum of GDL$_{(DME)}$ (Fig. 8a), where the main spectral features belong to TFSI⁻ and Li$_2$CO$_3$, except for the band at ~1000 cm^{-1} ascribable to the –Si–O–Si– bonds of the glass fiber separator and to other minor components in the –C–O–C– region[26] belonging to ether-derived byproducts on the CEI.

In Fig. 7c it is possible to observe that in the case of GDL$_{(TEGDME)}$, after cycling, large portions of this cathode are constituted by amorphous and likely organic material, which also appeared to be very sensitive to the electron beam of the SEM microscope. From the EDX mapping (Fig. 7d) and elemental quantification (Table 1) it was found that these regions are

fluorine-rich, with no remarkable sulfur content. This hints that these byproducts are derived from the cathode polymeric binder, which is polyvinylidene fluoride (PVDF). In fact, the absence of significant amounts of S suggests that the degradation of LiTFSI, the only other source of the fluorine apart from PVDF, is likely not involved at all in the formation of these deposits. The degradation of the polymeric binder leads to the loss of cathodic active material, *i.e.* carbon, in large parts of the cathode surface. The ATR-FTIR spectrum of GDL$_{(TEGDME)}$ is reported in Fig. 8b and shows signals that match those of PVDF and, to a minor extent, those of LiTFSI. The small amounts of sulfur that are related to the LiTFSI-derived byproducts appear to be located not in correspondence with the fluorine-rich deposits, but only on the remaining carbon surface (see Fig. S8). Overall, from the characterization of the cycled cathode, it is observed that the polymeric binder of the GDL is the cathode component that undergoes the majority of the undesired reactions occurring during the battery functioning.

The involvement of $^1O_2$ in the degradation processes occurring on GDL$_{(TEGDME)}$ is likely, since carbon and PVDF are usually stable towards the other reactive species such as superoxide and peroxide that are unavoidably formed during the battery operation in all the electrolyte formulations. This evidence is also in line with the recent findings of Zor *et al.*,[27] who reported no relevant $^1O_2$-related degradation of the electrolyte components. This implies that in the case of $^1O_2$ evolution, various cell components, including the electrode binder, are preferentially attacked.

The SEM images and EDX elemental maps of GDL$_{(DMSO)}$ are reported in Fig. 7e and f and confirm the accumulation of byproducts during the battery operation. The surface of the GDL is covered by a thick film-like layer mainly formed by the degradation of DMSO and secondarily TFSI⁻, according to the relative quantities of S and F detected by EDX elemental quantification (Table 1). The cathode–electrolyte interphase is composed of uniformly distributed sulfur and localized oxygen-rich regions (Fig. 7f). In the ATR-FTIR spectrum of GDL$_{(DMSO)}$
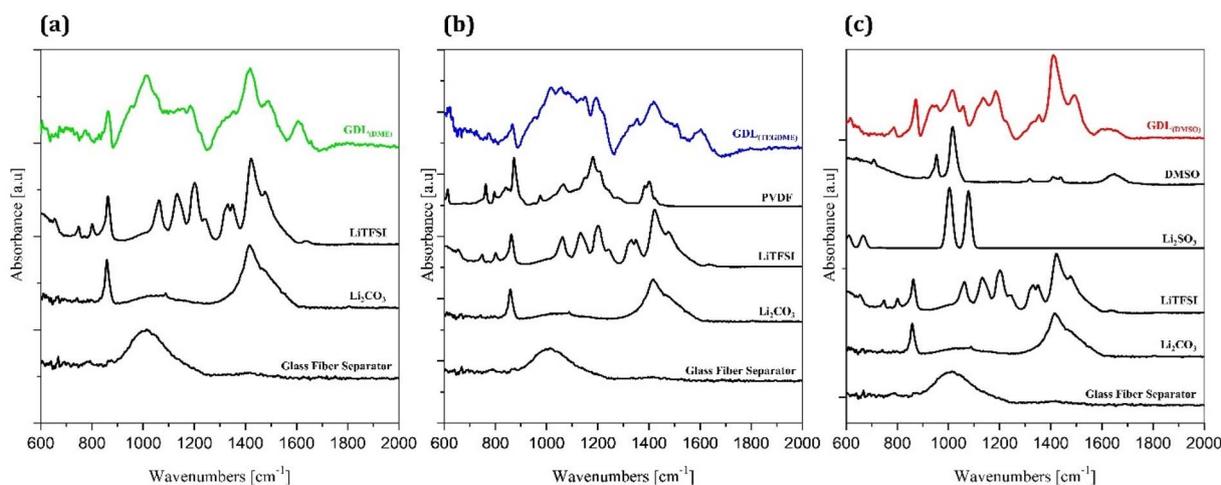

Fig. 8 ATR-FTIR spectra of (a) GDL$_{(DME)}$ and reference spectra of LiTFSI, Li$_2$CO$_3$ and the Whatman glass fiber separator. (b) GDL$_{(TEGDME)}$ and reference spectra of PVDF, LiTFSI, Li$_2$CO$_3$ and the Whatman glass fiber separator. (c) GDL$_{(DMSO)}$ and reference spectra of DMSO, Li$_2$SO$_3$ (theoretical), LiTFSI, Li$_2$CO$_3$ and the Whatman glass fiber separator.

566 | *J. Mater. Chem. A*, 2026, **14**, 560–569

This journal is © The Royal Society of Chemistry 2026

(Fig. 8c), the diagnostic signal of S=O stretching at 1044 cm^{-1} (ref. 28) is intense, indicating the presence of other DMSO-related byproducts. Among them, Li2SO3 is likely to be present since there are compatible peaks between 900 and 1100 cm−1 in the sample spectrum. The presence of dimethyl sulfide and methanesulfonic acid, the main byproducts expected by the Br$_2$ induced decomposition of DMSO,[25] is also compatible with the GDL$_{(DMSO)}$ spectrum as highlighted in Fig. S9.

Post-mortem characterization of the negative electrodes

Fig. 9 shows the morphology and elemental mapping obtained by SEM/EDX of Li metal anodes after cycling in different electrolytes, hereafter referred to as Li$_{(DME)}$, Li$_{(TEGDME)}$ and Li$_{(DMSO)}$.

In Fig. 9a, the SEM image of Li$_{(DME)}$ clearly shows anode deterioration in the presence of dendritic structures, indicating a less than optimal anode functioning in the DME-based electrolyte. In analogy with other Li metal battery systems, in Li–O$_2$ cells dendrites lead to Li detachment and loss of electrical contact that compromise the cell functioning, which simultaneously pose a severe safety hazard due to the possibility of short circuits.[29] The corresponding EDX elemental mapping in Fig. 9b indicates oxygen-rich regions, hinting that the degradation of the ether solvent occurred. The significant amounts of S and F on the Li surface (see Table 2) also indicate the presence of TFSI$^-$ fragments in the Solid Electrolyte Interphase (SEI).

The morphology of Li$_{(TEGDME)}$ in Fig. 9c appears different, showing predominantly mossy lithium. Thus, also in this case
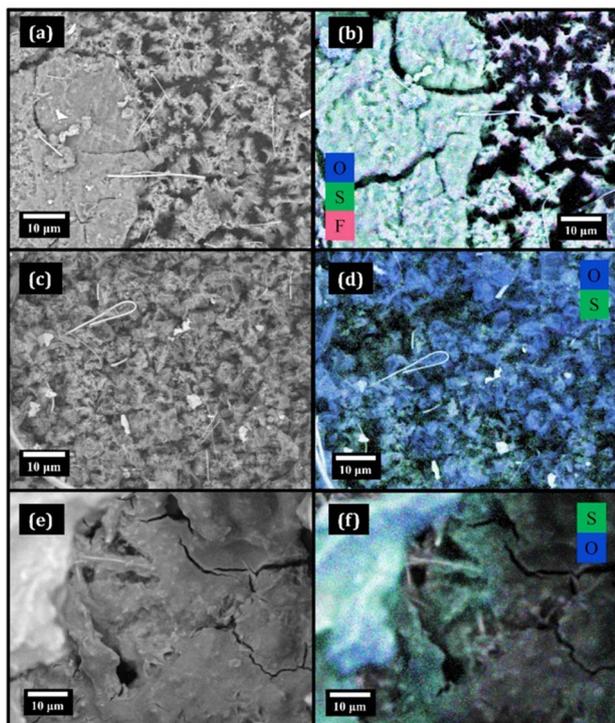

Fig. 9 Scanning electron microscopy images (5.000× magnification, working distance of 8.44 mm, 15 kV electron beam energy) of (a) Li$_{(DME)}$, (c) Li$_{(TEGDME)}$, and (e) Li$_{(DMSO)}$. Corresponding EDX elemental mapping of (b) Li$_{(DME)}$, (d) Li$_{(TEGDME)}$, and (f) Li$_{(DMSO)}$.

Table 2 EDX elemental quantitative analysis of lithium metal anodes cycled with different electrolyte formulations

Sample	Atomic%				
	C	O	S	F	Ni
Li$_{(DME)}$	36.09	16.58	10.67	32.10	3.49
Li$_{(TEGDME)}$	12.75	76.36	2.79	6.94	—
Li$_{(DMSO)}$	46.17	20.20	17.75	11.70	3.67

the uniformity of the Li morphology is compromised after the battery cycling, but the composition of the SEI layer is remarkably better with respect to the Li$_{(DME)}$ case. In fact, both the elemental mapping (Fig. 9d) and the quantitative analysis (Table 2) show oxygen as the major component. Usually, the presence of oxygen matches that of lithium, an element that cannot be detected by EDX spectroscopy. Thus, a rich and relatively uniform distribution of oxygen on the Li metal anode suggests the presence of a very thin SEI layer originating from byproducts formed by the reactions of Li with the electrolyte. Low amounts of S and F on the Li surface indicate mild TFSI$^-$ degradation that always occurs during the formation of the natural SEI layer on Li anodes. The improved stability of the TEGDME-based electrolyte towards Li metal compared to the DME case is explained by the TEGDME tendency to complex Li$^+$ within the LiTFSI ionic couple thanks to its longer chain.[30] This intermolecular interaction has already been demonstrated to play a key role in protecting the ether from oxidation,[31] *i.e.* the hydrogen abstraction from methylene groups by nucleophilic agents.[32]

The Li$_{(DMSO)}$ anode (Fig. 9e) shows some separator fibers that are incorporated in a thick film, mainly composed of S and O (Fig. 9f). Significant quantities of carbon are also present in the electrode surface (Table 2), supporting the occurrence of severe degradation of electrolyte components. As in the case of GDL$_{(DMSO)}$, the relative amount of S is higher than that of F, indicating that sulfur-containing byproducts derive mostly from DMSO. The Li metal anode appears consumed in the parasitic processes and covered with an insulating film that affects the reversibility of the plating/stripping processes.

Conclusion

Employing LiBr as a redox mediator in Li–O$_2$ batteries leads to radically different outcomes varying the solvent media. The optimal reversibility of cathodic reactions, *i.e.* ORR and OER, is obtained in DME, while critical issues arise in the other solvents, *i.e.* TEGDME and DMSO. The cathode functioning in TEGDME is affected by ^{1}O$_2$-induced parasitic processes. Conversely, in DMSO, LiBr redox mediation appears to follow a different mechanism allowing ^{1}O$_2$-free OER but, at the same time, enabling DMSO decomposition induced by Br$_2$. The Li metal anode functioning is not directly correlated with the cathode operation, since the worst Li morphology was found in the DME case. This implies that Li metal protection must be addressed independently.

In summary, our study underscores the critical role of solvent effects on the intricate interplay between the redox

This journal is © The Royal Society of Chemistry 2026

J. Mater. Chem. A, 2026, **14**, 560–569 | **567**

mediator, lithium superoxide (LiO_2), and the $TFSI^-$ anion in dictating singlet oxygen ($^1O_2$) release pathways in Li–O_2 batteries. It is well known that the choice of solvent significantly influences the solvation of these species, affecting the redox potentials, ion pairing, and overall electrochemical stability of the electrolyte. Specifically, the degree of Lewis acidity and basicity of the solvent, coupled with its dielectric constant, dictates the extent to which LiO_2 and $TFSI^-$ are solvated, subsequently influencing the reaction kinetics and the propensity for $^1O_2$ generation. A mismatch in the Lewis characteristics of the solvent and redox mediator can promote parasitic reactions and the formation of $^1O_2$, ultimately contributing to cell degradation. Understanding and tailoring the solvation environment is therefore crucial for suppressing $^1O_2$ formation and optimizing the performance and lifespan of Li–O_2 batteries. Therefore, the most promising approach for a reversible operation of an aprotic Li–O_2 battery is the employment of a RM with Lewis basicity contrasting the corresponding Lewis acidity of the electrolyte solvent, in parallel with a tailored Li metal protection strategy that limits the parasitic chemistries originating at the negative side.

Author contributions

All authors contributed equally to this work.

Conflicts of interest

There are no conflicts to declare.

Data availability

Data for this article, including raw spectral data, electrochemical data, and microscopy images, are available at SAPIENZA Open DATA, at **https://doi.org/10.13133/UNIROMA1/TAIQ8Y**.

Supplementary Information is available. See DOI: **https://doi.org/10.1039/d5ta04150c**.

Acknowledgements

References

1 W.-J. Kwak, Rosy, D. Sharon, C. Xia, H. Kim, L. R. Johnson, P. G. Bruce, L. F. Nazar, Y.-K. Sun, A. A. Frimer, M. Noked, S. A. Freunberger and D. Aurbach, Lithium-Oxygen Batteries and Related Systems: Potential, Status, and Future, *ACS Appl. Mater. Interfaces*, 2020, **120**(14), 6626–6683, DOI: **10.1021/acs.chemrev.9b00609**.

2 T. K. Zakharchenko, A. V. Sergeev, A. D. Bashkirov, P. Neklyudova, A. Cervellino, D. M. Itkis and L. V. Yashina, Homogeneous nucleation of Li_2O_2 under Li–O_2 battery discharge, *Nanoscale*, 2020, **12**, 4591–4601, DOI: **10.1039/C9NR08493B**.

3 A. Varzi, K. Thanner, R. Scipioni, D. Di Lecce, J. Hassoun, S. Dorfler, H. Altheus, S. Kaskel, C. Prehal and S. A. Freunberger, Current status and future perspectives of lithium metal batteries, *J. Power Sources*, 2020, **480**, 228803, DOI: **10.1016/j.jpowsour.2020.228803**.

4 A. Pierini, S. Brutti and E. Bodo, Reactive pathways toward parasitic release of singlet oxygen in metal-air batteries, *npj Comput. Mater.*, 2021, **71**(7), 1–8, DOI: **10.1038/s41524-021-00597-3**.

5 Z. Jiang, Y. Huang, Z. Zhu and F. Li, Quenching singlet oxygen via intersystem crossing for a stable Li-O₂ battery, *Proc. Natl. Acad. Sci., USA*, 2022, **119**(34), e2202835119, DOI: **10.1073/pnas.2202835119**.

6 Z. Jiang, B. Wen, Y. Huang, Y. Wang, H. Fang and F. Li, Heavy Atom-Induced Spin-Orbit Coupling to Quench Singlet Oxygen in a Li-O₂ Battery, *J. Am. Chem. Soc.*, 2025, **147**(13), 10992–10998.

7 Y. Chen, S. A. Freunberger, Z. Peng, O. Fontaine and P. G. Bruce, Charging a Li-O₂ battery using a redox mediator, *Nat. Chem.*, 2013, **5**, 489–494, DOI: **10.1038/nchem.1646**.

8 X. Gao, Y. Chen, L. R. Johnson, Z. P. Jovanov and P. G. Bruce, A rechargeable lithium–oxygen battery with dual mediators stabilizing the carbon cathode, *Nat. Energy*, 2017, **2**, 17118, DOI: **10.1038/nenergy.2017.118**.

9 C. Zhang, N. Dandu, S. Rastegar, S. N. Misal, Z. Hemmat, A. T. Ngo, L. A. Curtiss and A. Salehi-Khojin, A Comparative Study of Redox Mediators for Improved Performance of Li-Oxygen Batteries, *Adv. Energy Mater.*, 2020, **10**, 2000201, DOI: **10.1002/aenm.202000201**.

10 G. Leverick, S. Feng, P. Acosta, S. Acquaviva, F. Bardé, S. Cotte and Y. Shao-Horn, Tunable Redox Mediators for Li–O₂ Batteries Based on Interhalide Complexes, *ACS Appl. Mater. Interfaces*, 2022, **14**, 6689–6701, DOI: **10.1021/acsami.1c21905**.

11 A. Nakanishi, M. L. Thomas, H.-M. Kwon, Y. Kobayashi, R. Tatara, K. Ueno, K. Dokko and M. Watanabe, Electrolyte Composition in Li/O₂ Batteries with LiI Redox Mediators: Solvation Effects on Redox Potentials and Implications for Redox Shuttling, *J. Phys. Chem. C*, 2018, **122**, 1522–1534, DOI: **10.1021/acs.jpcc.7b11859**.

12 G. Leverick, M. Tułodziecki, R. Tatara, F. Bardé and Y. Shao-Horn, Solvent-Dependent Oxidizing Power of LiI Redox Couples for Li-O₂ Batteries, *Joule*, 2019, **3**, 1106–1126, DOI: **10.1016/j.joule.2018.12.014**.

13 A. Wang, X. Wu, Z. Zou, Y. Qiao, D. Wang, L. Xing, Y. Chen, Y. Lin, M. Avdeev and S. Shi, The Origin of Solvent Deprotonation in LiI-added Aprotic Electrolytes for Li-O₂

568 | *J. Mater. Chem. A*, 2026, **14**, 560–569

This journal is © The Royal Society of Chemistry 2026

Batteries, *Angew. Chem., Int.*, 2023, **62**(14), e202217354, DOI: **10.1002/anie.202217354**.

14 W.-J. Kwak, D. Hirshberg, D. Sharon, M. Afri, A. A. Frimer, H.-G. Jung, D. Aurbach and Y.-K. Sun, Li-O_2 cells with LiBr as an electrolyte and a redox mediator, *Energy Environ. Sci.*, 2016, **9**, 2334–2345, DOI: **10.1039/C6EE00700G**.

15 A. Pierini, A. Petrongari, V. Piacentini, S. Brutti and E. Bodo, A Computational Study on Halogen/Halide Redox Mediators and Their Role in $^1O_2$ Release in Aprotic Li-O_2 Batteries, *J. Phys. Chem. A*, 2023, **127**(44), 9229–9235, DOI: **10.1021/acs.jpca.3C05246**.

16 A. Petrongari, A. Pierini, V. Piacentini, P. Fattibene, C. De Angelis, E. Bodo and S. Brutti, Insights into the LiI Redox Mediation in Aprotic Li-O_2 Batteries: Solvation Effects and Singlet Oxygen Evolution, *ACS Appl. Mater. Interfaces*, 2023, **15**(51), 59348–59357, DOI: **10.1021/acsami.3c12330**.

17 C. F. Riadigos, R. Iglesias, M. A. Rivas and T. P. Iglesias, Permittivity and density of the systems (monoglyme, diglyme, triglyme, or tetraglyme + n-heptane) at several temperatures, *J. Chem. Thermodyn.*, 2011, **43**, 275–283, DOI: **10.1016/j.jct.2010.09.008**.

18 A. Ponrouch, E. Marchante, M. Courty, J. M. Tarascon and M. R. Palacín, In search of an optimized electrolyte for Na-ion batteries, *Energy Environ. Sci.*, 2012, **5**, 8572–8583, DOI: **10.1039/C2EE22258B**.

19 A. Jezuita, P. A. Wieczorkiewicz, H. Szatylowicz and T. M. Krygowski, Solvent effect on the stability and reverse substituent effect in nitropurine tautomers, *Symmetry*, 2021, **13**, 1223, DOI: **10.3390/sym13071223**.

20 J.-D. Chai and M. Head-Gordon, Long-range corrected hybrid density functionals with damped atom-atom dispersion corrections, *Phys. Chem. Chem. Phys.*, 2008, **10**, 6615–6620, DOI: **10.1039/B810189B**.

21 F. Neese, Software update: The ORCA program system—Version 5.0, *Wiley Interdiscip. Rev.: Comput. Mol. Sci.*, 2022, **12**, e1606, DOI: **10.1002/wcms.1606**.

22 A. Ahmadiparidari, S. Fuladi, L. Majidi, S. Plunkett, E. Sarnello, H. Gholivand, Z. Hemmat, S. Rastegar, S. N. Misal, N. Jimenez, P. C. Redfern, J. Wen, T. Li, A. T. Ngo, F. Khalili-Araghi, L. A. Curtiss and A. Salehi-Khojin, Enhancing the performance of lithium oxygen batteries through combining redox mediating salts with a lithium protecting salt, *J. Power Sources*, 2021, **491**, 229506, DOI: **10.1016/j.jpowsour.2021.229506**.

23 M. Lin, P. Archirel, N. Thi Van-Oanh, Y. Muroya, H. Fu, Y. Yan, R. Nagaishi, Y. Kumagai, Y. Katsumura and M. Mostafavi, Temperature dependent absorption spectra of Br^-, $Br_2^{\cdot}$, and Br_3^- in aqueous solutions, *J. Phys. Chem. A*, 2011, **115**, 4241–4247, DOI: **10.1021/jp1123103**.

24 W.-J. Kwak, H. Kim, H.-G. Jung, D. Aurbach and Y.-K. Sun, Review—A Comparative Evaluation of Redox Mediators for Li-O_2 Batteries: A Critical Review, *J. Electrochem. Soc.*, 2018, **165**, A2274–A2293, DOI: **10.1149/2.0901810jes**.

25 T. Aida, T. Akasaka, N. Furukawa and S. Oae, Catalytic Reduction of Sulfoxide by Bromine-Hydrogen Bromide System, *Bull. Chem. Soc. Jpn.*, 1976, **49**, 1117–1121, DOI: **10.1246/bcsj.49.1117**.

26 B. L. Papke, M. A. Ratner and D. F. Shriver, Vibrational spectroscopy and structure of polymer electrolytes, poly(ethylene oxide) complexes of alkali metal salts, *J. Phys. Chem. Solids*, 1981, **42**, 493–500, DOI: **10.1016/0022-3697(81)90030-5**.

27 C. Zor, K. D. Jones, G. J. Rees, S. Yang, A. Pateman, X. Gao, L. R. Johnson and P. G. Bruce, Singlet oxygen is not the main source of electrolyte degradation in lithium–oxygen batteries, *Energy Environ. Sci.*, 2024, **17**, 7355–7361, DOI: **10.1039/D4EE02176B**.

28 J. Ravi, A. Hills, E. Cerasoli, P. D. Rakowska and M. G. Ryadnov, FTIR markers of methionine oxidation for early detection of oxidized protein therapeutics, *Eur. Biophys. J.*, 2011, **40**, 339–345, DOI: **10.1007/s00249-010-0656-1**.

29 Y.-S. Hong, C.-Z. Zhao, Y. Xiao, R. Xu, J.-J. Xu, J.-Q. Huang, Q. Zhang, X. Yu and H. Li, Safe Lithium-Metal Anodes for Li-O_2 Batteries: From Fundamental Chemistry to Advanced Characterization and Effective Protection, *Batteries Supercaps*, 2019, **2**, 638–658, DOI: **10.1002/batt.201900031**.

30 B. D. Adams, R. Black, Z. Williams, R. Fernandes, M. Cuisinier, E. Jaemstorp Berg, P. Novak, G. K. Murphy and L. F. Nazar, Towards a Stable Organic Electrolyte for the Lithium Oxygen Battery, *Adv. Energy Mater.*, 2015, **5**, 1400867, DOI: **10.1002/aenm.201400867**.

31 S. Tsuzuki, W. Shinoda, S. Seki, Y. Umebayashi, K. Yoshida, K. Dokko and M. Watanabe, Intermolecular Interactions in Li+-glyme and Li+-glyme–TFSA− Complexes: Relationship with Physicochemical Properties of [Li(glyme)][TFSA] Ionic Liquids, *ChemPhysChem*, 2013, **14**, 1993–2001, DOI: **10.1002/cphc.201200843**.

32 M. Carboni, A. G. Marrani, R. Spezia and S. Brutti, 1,2-Dimethoxyethane Degradation Thermodynamics in Li–O2 Redox Environments, *Chem.–Eur. J.*, 2016, **22**, 17188–17203, DOI: **10.1002/chem.201602375**.

This journal is © The Royal Society of Chemistry 2026

J. Mater. Chem. A, 2026, **14**, 560–569 | **569**